Insights from dynamic models for an online flotation pulp sensor

E.C. Nienaber[1], K.S. Brooks[2], L. Auret[1,3]

[1] Stone Three, Somerset West, South Africa (ernst.nienaber@stonethree.com, lidia.auret@stonethree.com (ORCID: 0000-0002-2129-4971) – corresponding author)

[2] School of Chemical and Metallurgical Engineering, University of Witwatersrand, South Africa (kevin.brooks@wits.ac.za) (ORCID: 0000-0003-1939-142X)

[3] Department of Process Engineering, Stellenbosch University, Private Bag X1, Matieland, 7602, South Africa

It is well known that pulp-phase dynamics strongly impact flotation performance, but until recently online measurements of pulp behaviour were not possible. Stone Three have developed such an online pulp sensor (OPS) that performs in-situ machine vision to generate pulp measurements. A comparison of steady-state data from this sensor and the Anglo Platinum Bubble Sizer has been published, showing that the online pulp sensor produces measurements that are responsive to relevant process changes. These results highlighted that the exact calibration of the OPS requires more work. In this paper, the analysis is extended to empirical dynamic modelling of the OPS parameters, such as bubble size and superficial velocity, as functions of inputs including airflow, pulp level and reagent flows. The dynamic models provide good predictions of the bubble parameters and give insight into the effects of the input parameters on the intrinsic variables affecting the flotation performance. The dependence of concentrate grade and recovery on pulp parameters has been modelled for plants with online analysis. Where assays are used for grade and recovery analysis, online information on these performance indicators are not readily available. The models suggested in this work may prove valuable to link online pulp parameters to key performance indicators of the cell or bank, and these measurements may then be used for advisory systems and eventually closed-loop control.

Keywords: sensors and instrumentation; flotation; mineral processing; image processing

Introduction

Flotation in platinum group metal (PGM) concentrators is a challenging process to optimise, given the presence of many disturbances; control and recycle interactions between process units; as well as long delays between process performance measurements (recovery and grade of concentrate/tails) and manipulated variable effects (reagent dosing and regulatory control set points for pulp levels and air rate addition). Froth conditions have been monitored in real-time for several decades, but, until recently no robust real-time pulp condition measurements have been available. Recent developments in online pulp sensor technology are promising, since pulp sensor measurements can be an early indicator of cell flotation performance and extrapolate to bank and flotation section performance, making such measurements prime candidates for advisory systems, automatic control and optimization. One form in which pulp measurements can be integrated in automatic control is through dynamic models. State space modelling is a form of dynamic modelling that is typically used in control design and model-predictive control. Previous work has shown that the online pulp sensor measurements correspond to offline pulp characterization, specifically pulp sampling with the Anglo Platinum Bubble Sizer (within the constraints of biases from both sensors). This work shows the development of dynamic state space models relating manipulated variables to pulp measurements.

In the background section, a brief overview of flotation modelling is provided, with an emphasis on flotation pulp characteristics and flotation pulp/air measurements. The methodology section describes the experimental work, data processing and modelling procedure, while the results section presents the processed experimental data and the dynamic modelling results. Finally, conclusions and recommendations are made, together with discussions on future work and the potential of real-time pulp sensors.

Background

Froth flotation is a widely used minerals processing technique that processes roughly 9×10^9 tons of minerals annually. Wills and Napier-Munn (2005) stated “Flotation is undoubtedly the most important and versatile mineral processing technique, and both its use and application are continually being expanded to treat greater tonnages and to cover new areas.” With an exponential decline of high-grade ore bodies, flotation has permitted the mining of complex and low-grade ore bodies that would otherwise be regarded as uneconomic. As a concentration process, the objective is to separate valuable minerals from gangue or waste material.

Platinum is one of the major sources of revenue in South Africa with the bulk of the world's platinum group metal (PGM) production supplied from the country. With approximately 90% of the world's platinum reserves found in South Africa the country's mines supply an estimated 74% of the world's platinum demand (Jones, 1999). Platinum concentrators make extensive use of flotation banks, with primary and secondary roughers, scavengers, cleaners and recleaners in use. Total cells can number fifty or more.

The froth flotation process has attracted much interest, both from an academic research and industrial application perspective. The complex process of solid attachment to bubbles, enabled by reagents, followed by transport in a froth phase, is much better understood than previously. A convenient way of classifying the states found in a flotation cell is shown in Figure 1.

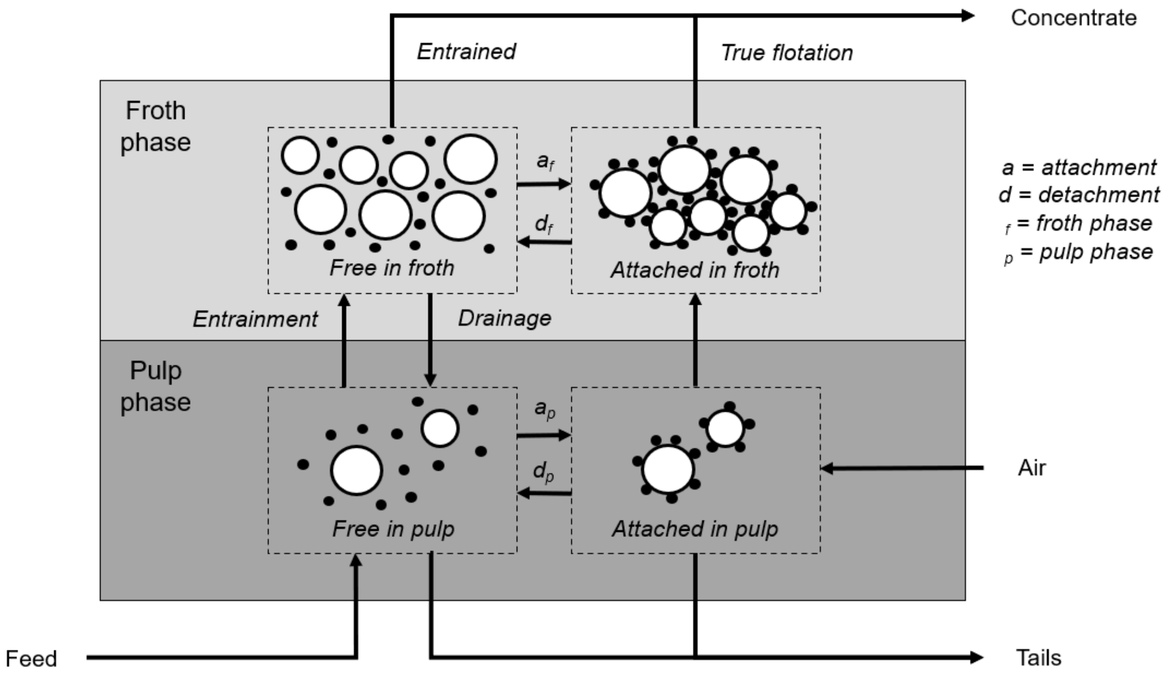

Figure 1: Representation of four states of bubble/particle interaction in a flotation cell: 1) free particles in the pulp phase; 2) attached particles in the pulp phase; 3) free particles in the froth phase and 4) attached particles in the froth phase (adapted from Quintanilla et al., 2021a)

It is clear from recent work that predictive models for flotation have to include both the pulp and the froth phase. Froth models consider the rate at which solids, water and air move between phases. Pulp phase models attempt to model the rate at which particles adhere to bubbles, and are then transported to the froth. These models often take the form of population balances, where the minerals and particles are divided into classes, and their distributions are used as input into a flotation rate model informed by chemical engineering reactor models. Some experimental work is needed to establish the rate constants needed for these models.

Measurements for monitoring and control of flotation cells and banks have been a challenge for the industry. Feed and airflow rates can be measured, together with the level of the interface between the froth and the pulp. Reagent flow rates can also be measured, although at times only a dosing pump speed is available. Online composition measurement remains relatively rare, although when in place it has proven to be useful for online control (Brooks and Koorts, 2014).

Cameras that are trained on the froth have been in use for some time (Aldrich et al., 2022). The camera image is passed through sophisticated image analysis algorithms, that can report quantities such as: absolute froth velocity, velocity towards the cell lip and froth direction; froth bubble size distribution statistics and colour analysis of the froth. Froth height can be measured with cameras using triangulation of a laser projection.

Measures of pulp bubble characteristics in froth flotation

The importance of the bubbles in the pulp phase in froth flotation has been recognised for many years (King, 1973, Bascur, 1982, Gorain, 1998). Many models relate the flotation rate to bubble characteristics in the pulp. The bubble characteristics used include (Quintanilla, 2021):

1. The Sauter mean bubble diameter for discrete class sizes:

$$\mathrm{d_{32}} = \frac{\sum_{\mathrm{i=1}}^{\mathrm{N_b}} \mathrm{n_i d_{BP_i}^3}}{\sum_{\mathrm{i=1}}^{\mathrm{N_b}} \mathrm{n_i d_{BP_i}^2}} \qquad [\,1\,]$$

Where d_{32} is the Sauter mean diameter, n_i is the number of bubbles in bin i, and d_i is the average diameter of the bubbles in bin i.

2. The superficial velocity found from the fundamental formula:

$$\mathrm{j_g} = \mathrm{u}\,\varepsilon_{\mathrm{g}} \qquad [\,2\,]$$

Where j_g is the superficial gas velocity, u is the bubble speed and ε_g is the gas holdup.

3. The bubble surface area flux is defined as:

$$\mathrm{S_b} = \frac{6\mathrm{J_g}}{\mathrm{d_{32}}} \qquad [\,3\,]$$

Where S_b is the bubble surface area flux.

Dynamic modelling of flotation

Quantanilla et al., (2021a) provide a comprehensive review of dynamic modelling specifically for froth flotation control, where the potential end-use of reported models is integration in online control systems, especially model predictive control (MPC). Empirical, phenomenological and hybrid (in the sense of continuous and discrete variables) models are discussed in detail in their review. Quantanilla et al. (2021a) remark that flotation modelling for control is challenging, due to the complexity of flotation and lack of reliable instrumentation. Their discussion of empirical models exclude traditional control engineering system identification models such as finite impulse response models (e.g., used to model froth velocities, grades and recoveries in a copper flotation plant by Brooks and Munalula (2017)) or other linear dynamic models (e.g., used to model final concentrate grades in a PGM flotation plant by Muller et al. (2010)) which can be estimated from data collected during plant step tests.

Pulp-air properties that appear in the dynamic models reviewed by Quantanilla et al. (2021a) include bubble surface area flux (phenomenological relation to superficial gas velocity and Sauter mean bubble diameter); gas hold up (phenomenological relation to bubble size distribution and bubble velocity, as well as empirical correlations from measured conductivity); Sauter mean bubble diameter (phenomenological relation to bubble size distribution as well as empirical correlation to superficial gas velocity) as well as bubble velocity (phenomenological relationship to bubble size distribution and gas holdup, amongst others). The dependence of these models on bubble size distribution is clear – typically, pulp bubble size distribution would be determined through sample-based pulp measurements (e.g., Quantanilla et al., 2021b), which are not available in real-time. The aforementioned empirical and phenomenological dynamic models would therefore be unable to accommodate operational changes in pulp bubble size distribution, leading to potential plant-model mismatch and subsequent sub-optimal control. This further motivates real-time measurements of pulp-air properties.

Flotation pulp sensors

Various sample-based and a few in situ techniques for flotation pulp-air property measurement have been reported in literature. Sample-based techniques include capillary systems with simple optical detectors (Tucker et al., 1994) as well as bigger sampling devices with built-in cameras (Chen et al., 2001; Harris et al., 2013; Vinnett et al., 2016). Current sample-based techniques are not appropriate for online control, given the manual work required in setting up the sampling equipment and the delay in measurements. Sample-based techniques for pulp-air property measurement are typically used in flotation plant surveys to determine optimal operating points (Harris et al., 2013). The Anglo Platinum Bubble Sizer (APBS) is a popular device for this application (Harris et al., 2013).

In situ techniques include acoustic methods (Spencer et al., 2011) and image-based methods (Horn et al., 2022; Maas et al., 2021). Maas et al. (2021) discuss an inline photo-optic measurement device demonstrated in a 5L bench scale batch flotation cell. Horn et al. (2022) discuss the Stone Three online pulp sensor and its application in operational flotation cells. Real-time in situ approaches to pulp-air measurement have the potential to provide valuable measurements for online control, given the direct measurement of in-pulp properties and higher sampling frequency that can be achieved in comparison to current sample-based techniques.

Online pulp sensor

The Stone Three online pulp sensor (illustrated in Figure 2) performs in situ machine vision analysis of the pulp. The online pulp sensor is designed to remain in situ for continuous real-time measurement, with occasional maintenance during scheduled plant shuts. Slurry abrasiveness keeps the lens clean, while LED lighting provides illumination. The recommended online pulp sensor immersion depth is similar to that of the Anglo Platinum Bubble Sizer: at least more than 30cm under the pulp-froth interface.

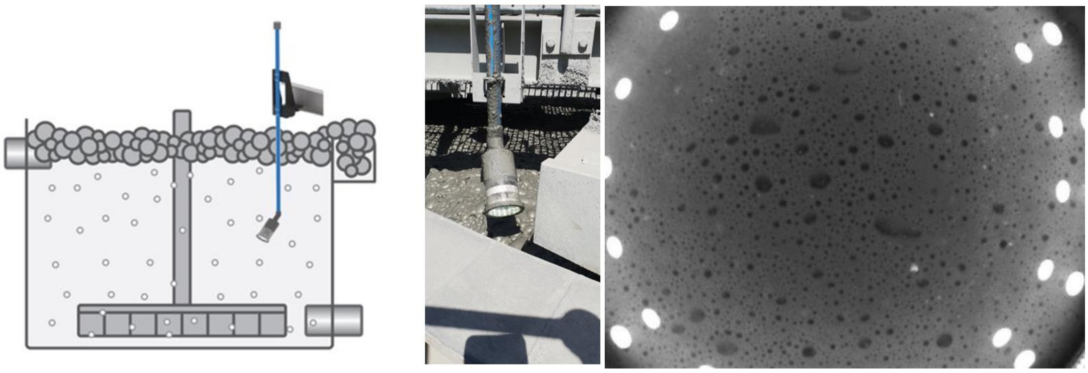

Figure 2: Schematic of online pulp sensor indicating position in a flotation cell (left); online pulp sensor before immersion (middle); example image captured by online pulp sensor (right).

Measurements available from the online pulp sensor include: Sauter mean bubble size, superficial gas velocity, gas hold up and average bubble rise velocity (Horn et al., 2022). Bubble size and gas hold up are determined through image processing of single images, while image processing of sequential images allows the estimation of bubble rise velocity, from which superficial gas velocity can be estimated (given gas hold up). Bubble surface area flux can also be inferred.

Methodology

Experimental design and data gathering

A Stone Three online pulp sensor was installed in a primary rougher cell in a PGM concentrator. An experiment was designed using a 3-factor Box-Behnken methodology to determine appropriate factor level combinations for the process factors: pulp level setpoint, cell sparging airflow setpoint and frother flow. Experimental runs were executed in random order, excepting centre runs, which were executed at the start, middle and end of the entire experiment duration in order to check for process drift. The duration of each experimental step was determined based on the observed process response – sufficient time was allowed for steady-state to be reached, but with an overall aim of keeping the entire experiment duration short to minimize operational disruption. Twenty experimental runs, each representing a step test, were executed over two days.

High-frequency data was collected through the process historian (setpoints and process values for pulp level and cell sparging airflow, frother reagent addition flowrate, bank feed volumetric flowrate, upstream primary mill feed and discharge density, at a sampling time of 10 seconds) and through the online pulp sensor data logging server (bubble velocity and bubble size statistics). The online pulp sensor sample time is variable, with a variable number of measurements that is available per minute, depending on the real-time image quality. Typical sample time for this study was 33 seconds.

Data preparation

Data preparation before dynamic model training included data selection (determining which time ranges to include), data resampling (downsampling to align the sampling frequencies of the process data and the online pulp sensor data) and data filtering (applying noise filters to smooth the time series data).

Data selection was based on the principle of excluding process upsets that would detrimentally affect model fitting. Process upsets were observed over the two days of testing, and considered carefully during data preparation: at the start of experimentation on day 1, a feed density disturbance was observed, as well as a disruption in frother flow. On day 2, an airflow abnormality occurred between 11:00 and 12:00 – airflow was switched off. Since dynamic modelling requires continuous periods of input and output data, the time range selected for modelling in this work spanned from day 1 (after the feed density and frother flow disturbances) to just before the airflow abnormality on day 2. Between step testing on day 1 and day 2, a period of about 12 hours represents normal process variation. This data was included in the analysis.

The data was resampled using a median resampling method to a communal sampling frequency of 10 seconds. A median operator is used instead of a mean operator, as the median is more robust to outliers. Linear interpolation is used to align the process historian and online pulp sensor data to the same time stamps. The sample size after data selection and data resampling is 7 621 samples per variable of interest, at a constant sample time of 10 seconds.

Noise removal was done using a first-order filter that was applied to all output measurements.

$$x_{filtered}(t) = \alpha \times x_{filtered}(t-1) + (1-\alpha) \times x_{raw}(t) \qquad [4]$$

Where: $x_{filtered}(t)$ is the filtered signal, $x_{raw}(t)$ is the raw/unfiltered signal (at time t), and $\alpha \in (0,1)$ is the filter factor. α is determined from the sampling frequency ΔT and a user-defined time constant τ (set to 100 seconds for this application):

$$\alpha = e^{-\frac{\Delta T}{\tau}} \qquad [5]$$

Dynamic modelling

An explicit discrete time-invariant state-space model (a traditional control engineering system identification model) is considered for the dynamic modelling of the effect of the process inputs on the pulp sensor measurements. The form of the discrete state-space model is given by:

$$\begin{aligned} \boldsymbol{x}(k+1) &= \boldsymbol{A}\boldsymbol{x}(k) + \boldsymbol{B}\boldsymbol{u}(k) \\ \boldsymbol{y}(k) &= \boldsymbol{C}\boldsymbol{x}(k) \end{aligned} \qquad [6]$$

Where: k is the time variable index, $\boldsymbol{x} \in \mathbb{R}^{n\times n}$ is the n-dimensional state vector (n is also the model order), $\boldsymbol{u} \in \mathbb{R}^{p\times n}$ is the p-dimensional input vector, $\boldsymbol{y} \in \mathbb{R}^{q\times n}$ is the q-dimensional output vector, and coefficient matrices $\boldsymbol{A} \in \mathbb{R}^{n\times n}, \boldsymbol{B} \in \mathbb{R}^{n\times p}$ and $\boldsymbol{C} \in \mathbb{R}^{q\times n}$ are the model parameters to be fit. For this application, $\boldsymbol{u} = [Pulp\ level; Air\ rate; Frotherflow]$ (i.e., $p = 3$) and $\boldsymbol{y} = \left[d_{32}; j_g; \varepsilon_g; u; S_b\right]$ (i.e., $q = 5$).

Given the time series data for $\boldsymbol{u}$ and $\boldsymbol{y}$, state-space dynamic model identification is achieved using canonical variate analysis in Aspen DMCplus® (Larimore, 1990). The model order n is a design parameter.

Model performance is quantitatively assessed by means of coefficient of determination (R^2) and normalised root mean square error metrics for each predicted variable (i.e., pulp sensor output). The robust equivalents of these performance metrics are also assessed.

$$R^2 = 1 - \frac{\sum_{i=1}^{N}(y_i - \hat{y}_i)^2}{\sum_{i=1}^{N}(y_i - \bar{y}_i)^2} \qquad [7]$$

Where: y_i is the actual/measured value of the output of interest for sample index i (with $i \in I$, where $I = \{i \in \mathbb{Z} | i \geq 0, i \leq N\}$), $\hat{y}_i$ is the predicted value of the output for sample index i, $\bar{y}$ is the mean of the N measurements of y_i. Note that a model may result in a negative coefficient of determination if the sum of squared model residuals for the model predictions (the numerator in the second term) is larger than the sum of squared residuals if the mean was used as a prediction (the denominator in the second term).

Another measure of model performance is the normalised root mean squared error $NRMSE$:

$$NRMSE = \frac{\sqrt{\frac{1}{N}\sum_{i=1}^{N}(y_i - \hat{y}_i)^2}}{y_{max} - y_{min}} \qquad [8]$$

The root mean squared error is normalised by the range of the actual process measurement (maximum y_{max} minus minimum y_{min}) to represent the fraction of the full range of the measured variable that constitute the root mean squared error.

Even though noise-filtering is applied, outliers can still be present in filtered process measurements. Robust statistics can be used to calculate model performance metrics after the most extreme mismatches between actual and predicted measurements are removed (the assumption here is that these extreme residuals may be attributed to outliers). Robust statistics have been used previously by authors assessing flotation model fits (Steyn and Sandrock, 2021). The residuals are defined as:

$$r_i = y_i - \hat{y}_i \qquad [9]$$

The absolute values of residuals $|r_i|$ are determined, and only samples $J = \{j \in I \| r_j| < r_{90}\}$ are retained for calculation of robust statistics, i.e., only sample indices where the residuals are smaller than the 90th percentile of $|r_i|$. The new sample size of the data is N_{90}. A robust coefficient of determination value (R_{90}^2) and robust normalised root mean squared error ($NRMSE_{90}$) may be calculated from the remaining sample indices $j \in J$.

$$R_{90}^2 = 1 - \frac{\sum_{j \in J}\left(y_j - \hat{y}_j\right)^2}{\sum_{j \in J}\left(y_j - \bar{y}_j\right)^2} \qquad [10]$$

$$NRMSE_{90} = \frac{\sqrt{\frac{1}{N_{90}}\sum_{j \in J}\left(y_j - \hat{y}_j\right)^2}}{y_{j,max} - y_{j,min}} \qquad [11]$$

Model performance is assessed visually by time-series plots (plotting actual and predicted values across time for the actual plant process variables).

Model interpretation is based on step response plots: for all p inputs, each input is stepped one at a time (while other inputs remain constant), and the effect on all q outputs are plotted. The dynamics of the effect of each input can be observed on all outputs (e.g., rise time, overshoot), as well as the final steady-state effect.

Where outputs are simulated, sufficient time is first provided such that an initial steady-state of the output variables can be achieved, before any input perturbation is introduced. This is relevant for both the simulation of step responses and the simulation of process response to the actual process inputs. For the latter case, the model predictions are aligned to the actual process responses by determining an appropriate bias term y_{bias} based on the first 30 samples (5 minutes) of operation.

$$y_{bias} = \frac{\sum_{i=1}^{30} y_i}{30} - \frac{\sum_{i=1}^{30} \hat{y}_i}{30} \qquad [\ 12\ ]$$

Results and discussion

Data preparation

Time series plots of the process factors and online pulp sensor metrics are shown in Figure 3. Note that actual values are omitted for confidentiality reasons. The step tests during day 1 and at the start of day 2 are evident in the input variables (pulp level, air rate and frother flow). The filtered pulp sensor measurements still exhibit noise, but responses to the steps in the input variables can be observed.

Dynamic modelling

The design parameter value (model order / number of states) that provided the best model fit was 10. The actual versus predicted pulp sensor time series for the full extent of the considered time period is given in Figure 4, while a zoomed in version focussing on the step tests on day 1 is shown in Figure 5.

From these figures, it is clear that although the model does not exactly predict the measured pulp properties, general trends in terms of direction of influence is captured. This is promising for potential control applications. The Sauter mean diameter shows the best predictability. The responses to the step changes on day 2 are not well-predicted, suggesting that other (unmodelled) disturbances may be affecting the pulp properties, and/or the presence of nonlinear effects that the state-space model cannot capture.

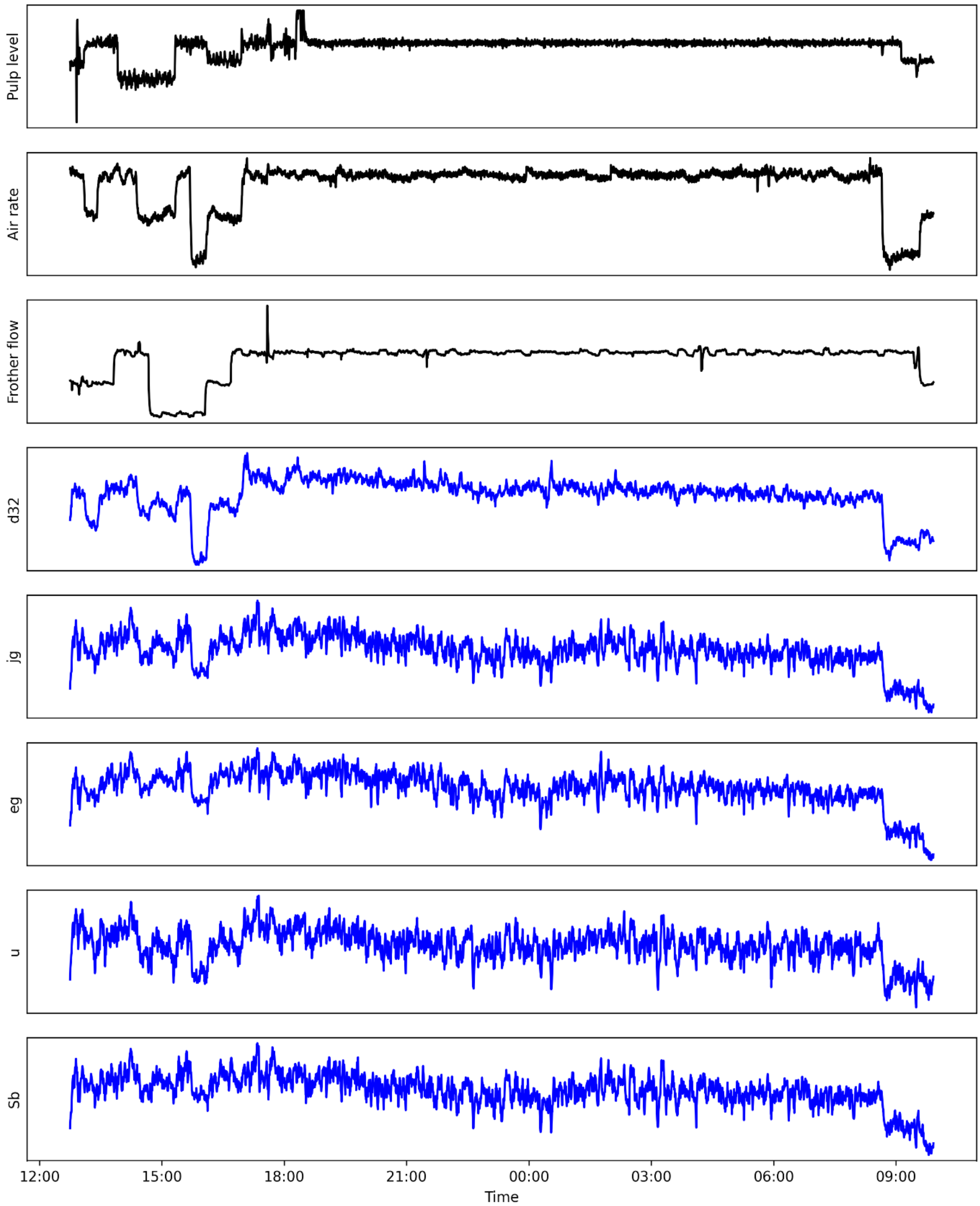

Figure 3: Time series plots for process factors (pulp level, airflow and frother flow) and filtered pulp sensor outputs (Sauter mean diameter, superficial gas velocity, gas hold up and bubble velocity).

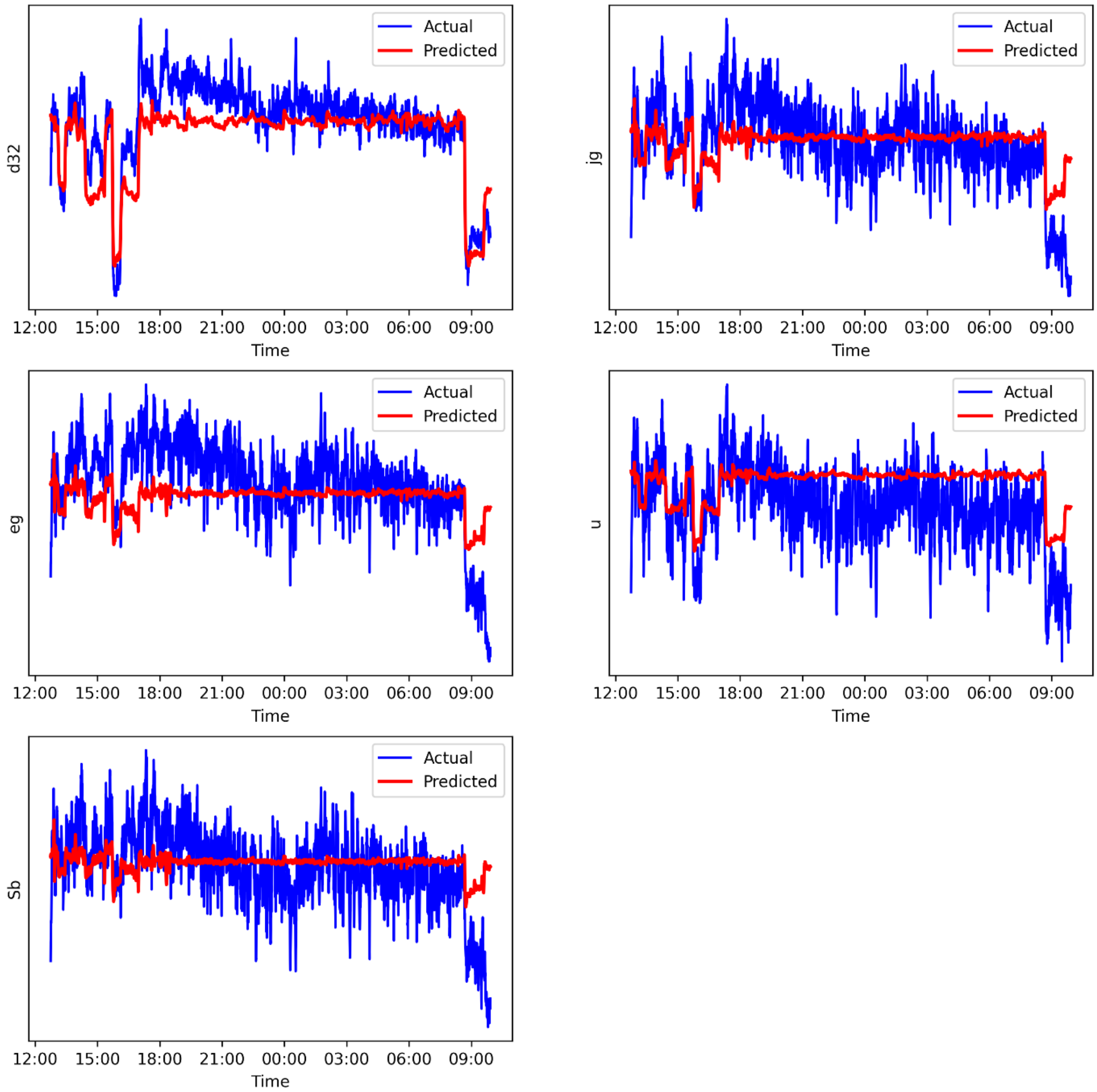

Figure 4: Time series plots for actual and predicted pulp sensor outputs (Sauter mean diameter, superficial gas velocity, gas hold up and bubble velocity).

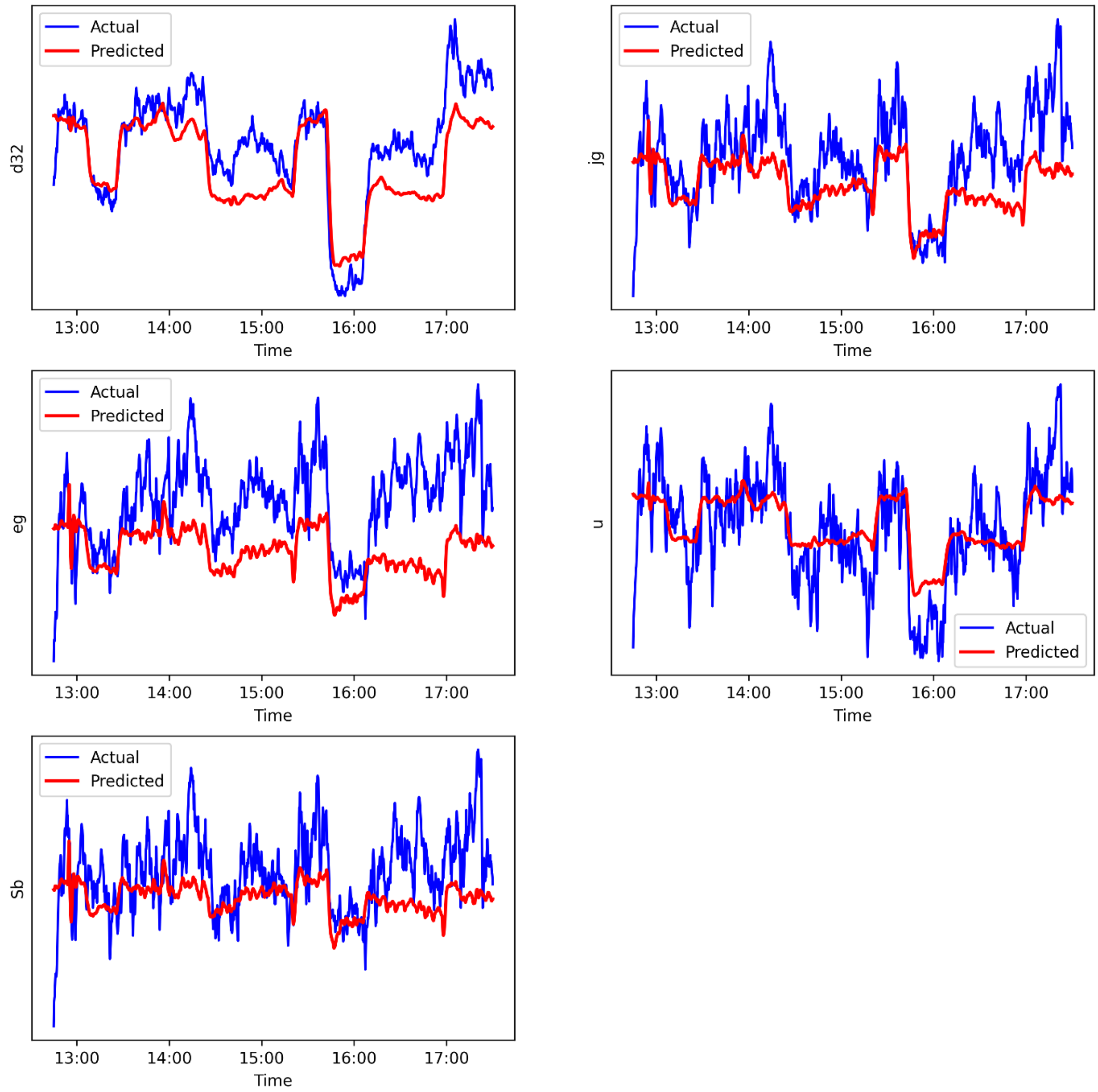

Figure 5: Time series plots for actual and predicted pulp sensor outputs (Sauter mean diameter, superficial gas velocity, gas hold up and bubble velocity) – zoomed in view of first five hours of experimentation.

Figure 6 presents the modelled responses for unit steps in the process inputs. (Note that interpretation of these responses should be seen within the context of the quality of the models, as can be gauged from the model prediction plots shown before, and the model performance metrics in Table 1).

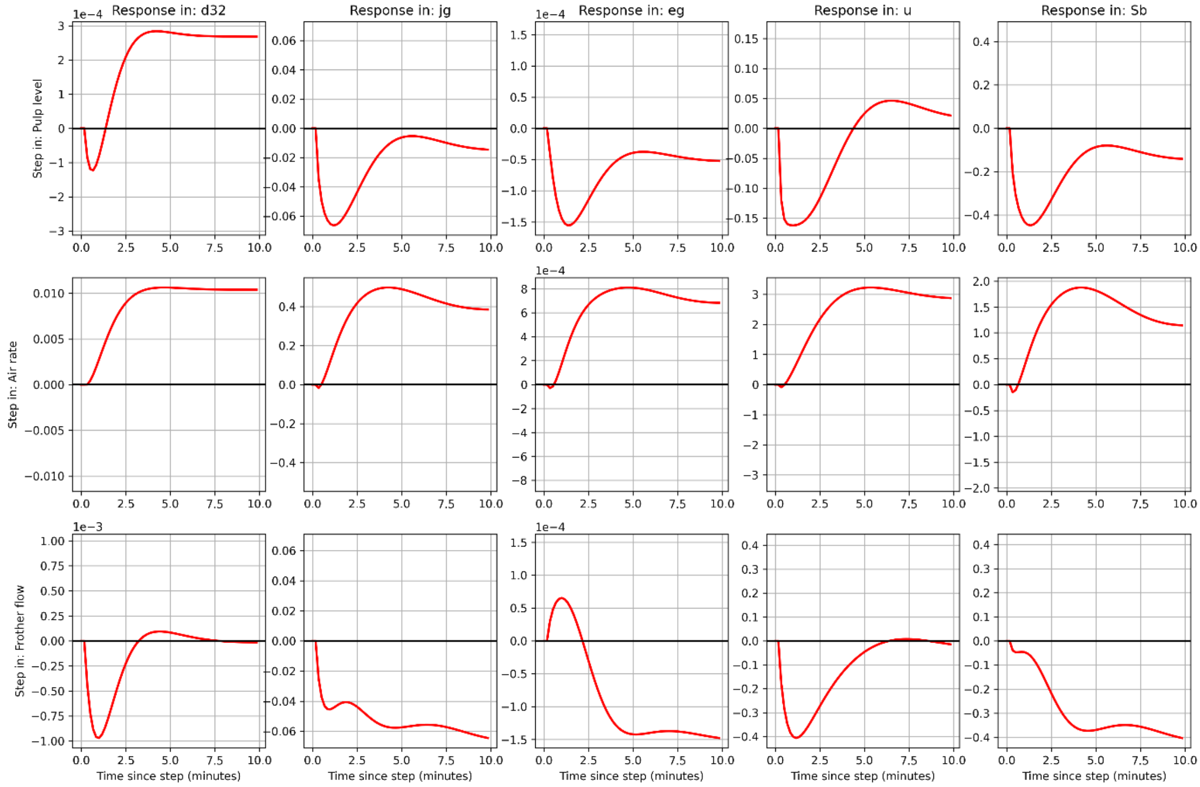

Figure 6: Modelled step response plots. Each row provides the results of input variables stepped in turn by one unit (pulp level, air rate and frother flow, respectively), with each row indicating the resulting response in the modelled pulp sensor outputs (Sauter mean diameter, superficial gas velocity, gas holdup and bubble velocity, respectively).

For a step increase in air rate, all modelled pulp measurements show positive responses, with similar rise times of around 3 minutes. The responses to air rate have the largest magnitude, as compared to step increases in pulp level or frother flow. These steady-state gain directions for air rate correspond to expected behaviour, while the rapid responses are of interest for designing controllers.

For a step increase in frother rate, the modelled pulp measurements show a range of different dynamics, including an inverse response (gas holdup). The response of Sauter mean diameter to the frother flow is interesting – a fast (within 1 minute) initial decrease, followed by a return to initial conditions. The initial decrease in bubble size is related to expected behaviour of frothers, while the lack of a lasting effect may indicate that the operational data on which the model is built represents process conditions close to the critical coalescence concentration of the frother. In contrast, superficial gas velocity shows a sustained decrease for a step increase in frother flow.

The modelled responses of pulp variables to a step increase in pulp level show complex dynamics (inverse response for Sauter mean diameter and bubble velocity, as well as overshoots for the remaining pulp variables), with no readily accessible interpretation from a phenomenological perspective.

The quantitative model evaluation metrics are provided in Table 1 (note that these metrics were evaluated on the same data as used for model training).

Table 1: Model training evaluation metrics

	R^2	R^2_{90}	$NRMSE$	$NRMSE_{90}$
d_{32}	0.63	0.76	0.10	0.09
j_g	0.30	0.34	0.12	0.13
ε_g	0.12	0.12	0.14	0.16
u	-0.07	0.03	0.15	0.16
S_b	0.14	0.11	0.13	0.15

The best-modelled response in terms of quantitative model evaluation metrics is for Sauter mean diameter, with the model capturing potentially valuable variability for superficial gas velocity. The other responses show poor model evaluation metrics. Bubble velocity stands out, with a negative coefficient of determination value (suggesting that the mean of bubble velocity is a better prediction model than the state-space model).

Given that phenomenological and empirical correlations exist (Quintanilla et al., 2021a) that incorporate pulp bubble size distribution and Sauter mean diameter, the potential exists to integrate the dynamic state-space model predictions of Sauter mean diameter (which shows good model performance) with such correlations to improve prediction performance.

Conclusions

This work has demonstrated the feasibility of empirical dynamic models for pulp-phase properties, with good model performance observed for Sauter mean bubble diameter in response to changes in pulp level, air rate and frother flow. Qualitative dynamic trends could also be captured for superficial gas velocity, gas hold up, specific bubble area flux and bubble velocity. Overall, pulp conditions respond quickly (within 5 minutes) to changes in the investigated process inputs.

Future work will include the incorporation of measured process disturbances (such as feed density and feed rate) into the state-space model, and demonstrate the potential benefits on online pulp measurements through quicker disturbance mitigation with model predictive control. The state-space model can also be integrated with existing phenomenological and empirical correlations for pulp phase predictions, and further connected to froth phase modelling and froth phase measurements (e.g., froth bubble distribution and froth velocity).

The integration of online pulp measurements in advanced process control may provide benefits not only for disturbance mitigation, but also as part of an optimization control layer (given the link of pulp and froth conditions to cell and bank recovery).

Acknowledgements

The authors would like to thank the co-operation and assistance provided by Anglo American Platinum for enabling this work to be performed and ensuring testing could be carried out on an operational concentrator. Specific thanks to Chris Steyn and the operators and metallurgists at the concentrator.

References

Aldrich, C., Avelar, E., Liu, X., 2022. Recent advances in flotation froth image analysis. Minerals Engineering, Vol 188, 107823. 10.1016/j.mineng.2022.107823

Bascur, O.A., Herbst, J.A., 1982. Dynamic modelling of a flotation cell with a view toward automatic control. CIM Bulletin, Vol 75(845), pp. 76-76.

Brooks, K.S., Koorts, R., 2014. Model predictive control of a zinc flotation bank using online X-ray fluorescence analysers. IFAC PapersOnline, Vol 50 (1), pp. 10214-10219. 10.1016/j.ifacol.2017.08.1772

Brooks, K.S., Munalula, W., 2017. Flotation velocity and grade control using cascaded model predictive control. IFAC PapersOnline, Vol. 50 (2), pp. 25-30. 10.1016/j.ifacol.2017.12.005

Chen, F., Gomez, C.O., Finch, J.A., 2001. Technical note: Bubble size measurement in flotation machines. Minerals Engineering, Vol. 14 (No. 4), pp. 427-432. 10.1016/S0892-6875(01)00023-1

Gorain, B.K., Franzidis, J.P., Manlapig, E.V., 1997. Studies on impeller type, impeller speed and air flow rate in an industrial scale flotation cell. Part 4: Effect of bubble surface area flux on floatation performance. Minerals Engineering, Vol. 10, pp. 367-379. 10.1016/S0892-6875(97)00014-9

Gorain, B.K., Napier-Munn, T.J., Franzidis, J.P., Manlapig, E.V., 1998. Studies on impeller type, impeller speed and air flow rate in an industrial scale flotation cell. Part 5: Validation of k-Sb relationship and effect of froth depth. Minerals Engineering, Vol. 11(7), pp. 615-626. 10.1016/S0892-6875(98)00046-6

Harris, A., Venkatesan, L., Greyling, M., 2013. A practical approach to plant-scale flotation optimization. Journal of the Southern African Institute of Mining and Metallurgy, Vol. 113 (No 3), pp. 263-272.

Horn, Z.C., Haasbroek, A.L., Nienaber, E.C., Auret, L., Brooks, K.S. 2022. Comparison of online and offline pulp sensor metrics in an industrial setting. IFAC PapersOnLine, Vol. 55 (21), pp. 91-96. 10.1016/j.ifacol.2022.09.249.

Jones, R. T., 1999. Platinum smelting in South Africa. South African Journal of Science, 95, 525-534.

King, R.P., 1973. Model for the design and control of flotation plants. Mintek.

Larimore, W. E., 1990. Canonical variate analysis in identification, filtering, and adaptive control. In 29th IEEE Conference on Decision and control (pp. 596-604). IEEE.

Maas, S., Sweet, J., Venkatesan, L., Shabalala, N., Finfer, D., Dutton, J. 2021. Application of an endoscopic device for in situ hydrodynamic measurements. Flotation ’21, Online conference, November 8-12, 2021.

Muller, D., De Villiers, P.G.R., Humphries, G., 2010. A holistic approach to flotation mass pull and grade control. IFAC Proceedings Volumes, Vol 43(9). Pp. 133-136. 10.3182/20100802-3-ZA-2014.00031

Quantanilla, P., Neethling, S.J., Brito-Parada, P.R., 2021a. Modelling for froth flotation control: A review. Minerals Engineering, Vol 162. 106718. 10.1016/j.mineng.2020.106718.

Quantanilla, P., Neethling, S.J., Navia, D., Brito-Parada, P.R., 2021b. A dynamic flotation model for predictive control incorporating froth physics. Part I: Model development. Minerals Engineering, Vol 173. 107192. 10.1016/j.mineng.2021.107192

Spencer, S.J., Bruniges, R., Roberts, G., Sharp, V., Catanzo, A., Bruckard, W., Davey, K., Zhang, W., 2012. An Acoustic Technique for Measurement of Bubble Solids Mass Loading: (b) Monitoring of Jameson Cell Flotation Performance by Passive Acoustic Emissions. Minerals Engineering, Vol 36-38. pp.21-30. 10.1016/j.mineng.2012.02.011

Steyn, C., Sandrock, C., 2021. Causal model of an industrial platinum flotation circuit. Control Engineering Practice, Vol 109, 104736. 10.1016/j.conengprac.2021.104736

Tucker, J.P., Deglon, D.A., Franzidis, J.P., Harris, M.C., O’Connor, C.T., 1994. Evaluation of a direct method of bubble size distribution measurement in a laboratory batch flotation cell. Mineral Engineering, Vol. 7. pp. 667-680. 10.1016/0892-6875(94)90098-1

Vinnett, L., Ledezma, T., Alvarez-Silva, M., Waters, K., 2016. Gas holdup estimation in flotation machines using image techniques and superficial gas velocity. Minerals Engineering, Vol. 96-97, pp.26-32. 10.1016/j.mineng.2016.07.005

Wills, B.A., Napier-Munn, T., 2005. Froth Flotation. In: Wills' Mineral Processing Technology. Elsevier, pp. 257-352.

Zhang, W., Spencer, S.J. & Coghill, P., 2012. An acoustic technique for measurement of bubble solids mass loadings – (a) Fundamental study of single bubble. Minerals Engineering, Vol. 36-38, pp. 45-52. 10.1016/j.mineng.2012.02.007

Appendix

The state-space coefficient matrices fitted to the process data are provided in the following tables. The sample time for the discrete time-invariant model is 10 seconds.

Table 2: State-space model coefficient matrix ***A***

9.79E-01	-4.02E-03	-7.56E-03	-3.47E-02	-8.19E-02	1.99E-02	-1.99E-03	-1.96E-02	-9.83E-03	2.72E-02
5.04E-03	9.47E-01	-1.61E-02	1.46E-03	-1.33E-02	-3.80E-02	-1.19E-01	3.52E-02	-3.48E-02	3.66E-03
2.08E-04	2.88E-02	8.82E-01	1.77E-02	4.10E-03	-2.47E-01	2.45E-02	-7.63E-02	3.42E-02	3.63E-02
3.52E-02	1.42E-04	1.48E-02	8.95E-01	2.58E-03	9.52E-02	-5.24E-02	-1.77E-03	1.01E-01	3.32E-02
7.87E-02	2.05E-02	-1.09E-03	-8.82E-03	8.81E-01	7.41E-02	-6.26E-02	-5.55E-02	-2.07E-02	-6.83E-02
-2.68E-03	-1.30E-02	2.65E-02	1.89E-02	-6.83E-03	3.36E-01	3.01E-01	2.31E-01	9.38E-02	-1.34E-02
-2.95E-02	1.41E-01	-5.10E-03	2.89E-02	8.63E-03	1.22E-02	6.79E-01	-2.69E-02	2.29E-02	1.34E-02
-4.07E-03	-1.17E-02	6.23E-02	-4.69E-03	2.29E-02	4.17E-02	-1.23E-01	7.21E-01	-3.47E-02	9.30E-02
5.44E-03	5.77E-02	-3.27E-03	-1.13E-01	4.29E-02	1.41E-01	-1.01E-01	-1.27E-01	8.15E-01	4.46E-02
-2.69E-02	-1.40E-02	1.04E-02	-5.75E-02	3.12E-02	9.08E-02	-3.47E-02	-2.03E-02	-6.84E-02	8.35E-01

Table 3: State-space model coefficient matrix ***B***

-1.37E-02	-7.13E-03	9.13E-03
1.14E-02	-3.16E-02	-5.75E-03
8.59E-02	-7.70E-02	2.87E-01
-4.60E-02	1.74E-02	-8.39E-02
-4.70E-02	-3.47E-02	-4.50E-02
3.38E-01	1.04E-01	2.95E-01
-5.07E-02	-4.68E-01	-2.23E-02
-8.05E-02	-6.83E-02	2.45E-01
-9.89E-02	-6.05E-02	2.14E-02
-4.40E-02	-2.37E-02	-1.32E-01

Table 4: State-space model coefficient matrix ***C***

-1.56E-03	6.56E-03	-2.77E-04	4.13E-03	-5.90E-04	3.38E-05	-2.26E-04	7.11E-05	6.82E-05	1.31E-04
-3.73E-01	4.41E-02	2.38E-01	7.56E-01	6.56E-01	1.69E-02	-1.72E-02	-1.40E-02	2.82E-02	-6.37E-03
-5.20E-04	-9.01E-07	7.73E-04	1.89E-03	5.76E-04	1.43E-05	-3.29E-05	-2.95E-05	8.24E-05	1.57E-05
-3.78E+00	2.75E-01	4.03E-01	1.26E+00	3.76E+00	4.76E-02	-5.53E-02	-4.89E-02	2.81E-02	-1.03E-01
-2.34E+00	-6.26E-01	1.90E+00	4.43E+00	4.60E+00	8.51E-02	-8.03E-02	-1.10E-01	1.79E-01	-6.48E-02